wavenumber pair of ν(CO) absorptions, whereas in the IR spectrum of **3** the intensity of this pair has been reduced almost to zero. This lends further support to the notion that this upper pair of ν(CO) absorptions belongs to the η^2-isomer. The correctness of this assignment is, of course, crucial to the arguments presented in this paper. There is no evidence that it should be otherwise and considerable evidence in its favor.

Conclusions

It has been demonstrated that the azobenzene ligand is bound in the η^2-form (**1a**) in the crystal structure of $CpRe(CO)_2(N_2Ph_2)$ (**1**). In solution, IR and NMR spectroscopic data have been interpreted as evidence for both η^2- (**1a**) and η^1-coordinated (**1b**) azobenzene complexes in equilibrium, with the η^1-form undergoing coordination site shift, probably via the same η^2-form that is observed in the crystal structure, and with the η^2-form undergoing further fluxional behavior, which is likely to be inversion at each nitrogen atom. This appears to be the first demonstration of a η^1-η^2 coordination shift in diazene chemistry.

Acknowledgment. This work was supported by the NSERC, Canada, through operating grants to D.S. and F.W.B.E. We thank Dr. A. S. Tracey for assistance with the NOE and saturation transfer studies.

Supplementary Material Available: Anisotropic thermal parameters (Table S1), calculated hydrogen atom coordinates (Table S2), calculated mean planes and dihedral angles (Table S3), and $^{13}C\{^1H\}$NMR spectra of **1** at 221 K (Figure 4c) and 200 K (Figure 4d) (6 pages); calculated and observed structure factors (Table S4) (8 pages). Ordering information is given on any current masthead page.

Contribution from the Department of Chemistry and Materials Science Center, Cornell University, Ithaca, New York 14853

Tin Sulfide, $(Te_2)_2I_2$, and Related Compounds: Symmetry-Controlled Deformations in Solid-State Materials

Wolfgang Tremel[1] and Roald Hoffmann*

Received June 6, 1986

The layered compound SnS normally adopts the GeS structure but is also observed to undergo a second-order phase transition to the more symmetric TlI structure close to the melting point. GeS and TlI, however, prefer the distorted low-temperature or the undistorted high-temperature structure, respectively, at ambient pressure. The band structures for both SnS modifications are constructed, and in a 2-dimensional picture the distortion can be traced to a mixing of the conduction band into the valence band, similar to a second-order Jahn-Teller distortion. The band gap (or the relative electronegativities) determines whether the distortion occurs. The derived picture can be used to analyze the electronic structure of related compounds, such as $(Te_2)_2I_2$, InS, or HgCl.

The solid-state structures of 10-electron (per two atoms) compounds can be related to the rock salt structure by a successive bond-breaking process. Burdett and McLarnan[2] have given an enumeration of the resulting structures. While the As[3] or GeTe[4] structure types arise from a rhombohedral distortion, a quasi-tetragonal distortion leads to the structure of black P[5] or GeS[6] (**1**). This deformation transforms six "bonds" in the NaCl

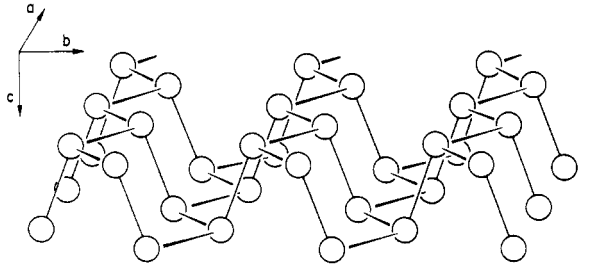

1

structure into three bonds in the GeS structure. Both Ge and S atoms have three neighbors at somewhat shorter (2.7 Å) and longer (3.3 Å) distances, so that GeS could be viewed as a distorted rock salt structure. Actually phosphorus is known to transform under high pressure to a rock salt modification.[7]

In and Tl halides are isoelectronic with group IV (group 14[40]) chalcogenides, although their structure looks different.[8] It can be built up, however, by stacking double layers from the NaCl structure, where consecutive layers are shifted due to the stereochemically active electron lone pairs. This is depicted schematically in **2**. Every atom has 1 + 4 neighbors making up a

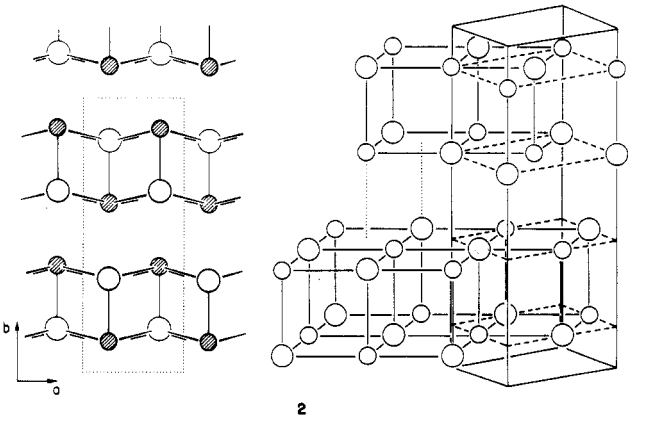

2

distorted octahedron with one unoccupied position. There is a little buckling of alternate pairs of atoms in one direction, so that the cations project out of the layer. Interestingly enough SnS and SnSe were found to undergo a structural transformation from the GeS to the TlI type, as shown in **3**. The phase transition takes place just below the melting point, and it is a second-order transition.[9]

(1) DAAD/NATO Postdoctoral Fellow 1984-1985, DFG Fellow 1985-1986. Present address: Anorganisch-Chemisches Institut der Universität Münster, D4400 Münster, Federal Republic of Germany.
(2) Burdett, J. K.; McLarnan, T. *J. Chem. Phys.* **1981**, *75*, 5764.
(3) Schieferl, D.; Barrett, C. S. *J. Appl. Crystallogr.* **1969**, *2*, 905.
(4) (a) Schubert, K.; Fricke, H. *Z. Metallkd.* **1953**, *44*, 457. (b) Goldak, J.; Barrett, C. S. *J. Chem. Phys.* **1966**, *44*, 3323.
(5) Brown, A.; Rundqvist, S. *Acta Crystallogr.* **1965**, *19*, 684.
(6) GeS: Zachariasen, W. H. *Phys. Rev.* **1932**, *40*, 917. Wiedemeier, H.; von Schnering, H.-G. *Z. Kristallogr.* **1978**, *148*, 295. GeSe: Dutta, N. S.; Jeffrey, G. A. *Inorg. Chem.* **1965**, *4*, 1363. SnS: Hofmann, W. *Z. Kristallogr. Kristallgeom., Kristallphys., Kristallchem.* **1935**, *92A*, 161. SnSe: Ohazaki, A.; Ueda, I. *J. Phys. Soc. Jpn.* **1956**, *11*, 470.
(7) Jamieson, J. C. *Science (Washington, D.C.)* **1963**, *139*, 762, 1291; **1964**, *140*, 72.
(8) Helmholtz, L. *Z. Kristallogr. Kristallgeom., Kristallphys., Kristallchem.* **1956**, *95A*, 129.

0020-1669/87/1326-0118$01.50/0

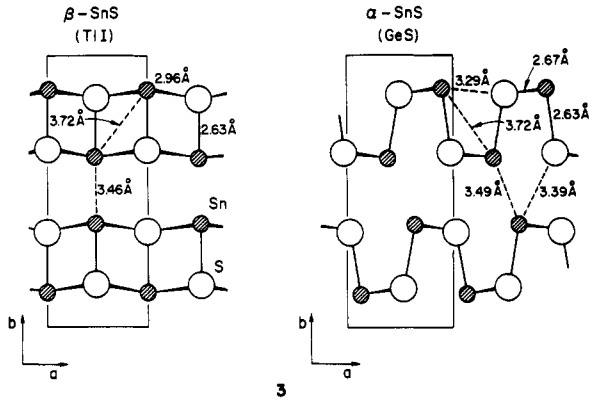

3

We would like to understand the origin for the observed structural distortion in SnS. Some general statements can be made structurally and electronically about this transformation. The packing of the layers relative to each other is hardly different, but within each double double layer there is a change from a 3 + 2 to a 1 + 4 coordination. A bond order of $n = 0.5$ can be assigned to the four longer bonds by using Pauling's relation.[10] This value is easy to rationalize if we assume hypervalent bonding for the pyramidal SnS_5^{8-} fragments. For the axial bond there is one bonding electron pair; for the basal bonds two bonding electron pairs are shared between four bonds. The situation is shown schematically for SnH_5^{3-} in interaction diagram **4**. On the left

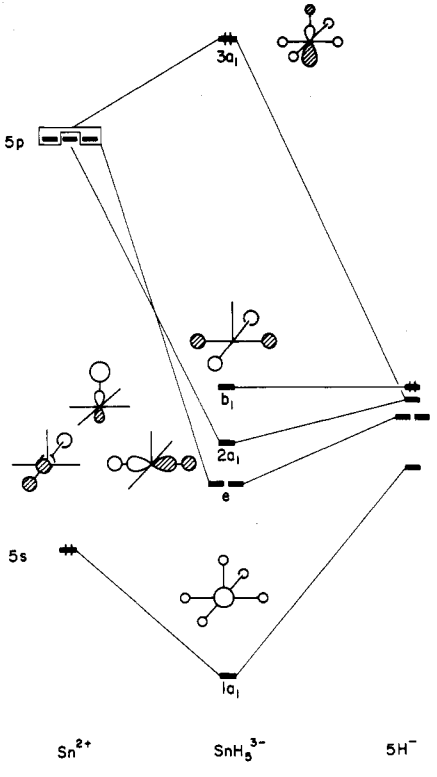

4

are given the orbitals of Sn^{2+}, which transform as $2a_1 + e$ under C_{4v} symmetry. On the right are the orbitals of $5H^-$, which transform as $2a_1 + b_1 + e$. An important feature is that the b_1 combination on the right finds no Sn orbital to interact with and remains completely ligand located and, therefore, Sn–H nonbonding. The b_1 orbital is derived from the e_g set of an octahedral SnH_6^{4-} unit (as is the $3a_1$ orbital in the SnH_5^{3-} composite). So, the SnH_5^{3-} fragment has four equatorial bonding orbitals, but only two bonding electron pairs. For the axial bond, there is one bonding electron pair, which corresponds to a full Sn–H bond. The $3a_1$ orbital in **4** has a large contribution not only from central atom s and ligand orbitals but also from central atom p_z and axial ligand contributions. As a result of the p_z mixing, a lone pair ($3a_1$) is created, pointing to the vacant coordination site. Next, two cis equatorial H^- ligands are pulled off one by one. The evolution of the fragment orbitals is shown in **5**. We are left finally in a

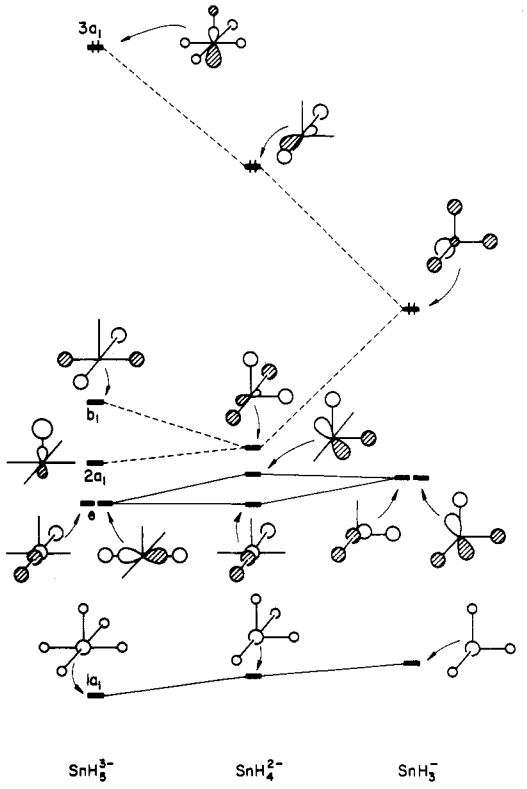

5

situation which is familiar from simple AH_3 molecules. For SnH_3^- on the right-hand side, there are bonding electron pairs for three bonds and one lone pair located on the tin atom. This matches the picture we see in SnS (GeS modification).

There are two simple ways to construct the individual layers in the TlI structure, and we are going to use these ways of geometrical construction to analyze the band structure as well. Following the hierarchy of interactions, we may start with a diatomic SnS monomer, which is surrounded by four other SnS units (generated by the glide planes perpendicular to *b*) pointing in the opposite direction, as shown in **6**. This picture describes

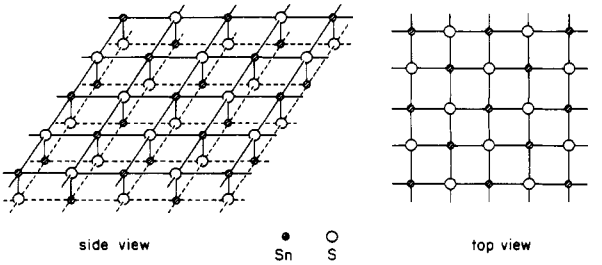

6

the layers as aggregated SnS units. In an alternative way, the SnS layers may be constructed from an AB stacking of slightly

(9) (a) Wiedemeier, H.; Csielag, F. J. *Z. Kristallogr.* **1979**, *149*, 17. (b) von Schnering, H.-G.; Wiedemeier, H. *Z. Kristallogr.* **1981**, *156*, 143. (c) Bucchia, P. S. D.; Jumas, J.-C.; Maurin, M. *Acta Crystallogr., Sect. B; Struct. Crystallogr. Cryst. Chem.* **1981**, *B37*, 1903. (d) Chattopadhyay, T.; Pannetier, J.; von Schnering, H.-G. *Z. Kristallogr.* **1985**, *151*, 29. (e) Chattopadhyay, T.; Pannetier, J.; von Schnering, H.-G. *J. Phys. Chem. Solids* **1986**, *47*, 879. For a general reference on second-order phase transitions see: Landau, L. D.; Lifshitz, E. M. *Statistical Physics*; Pergamon: London, 1959. See also: Franzen, H. F. *Lect. Notes Chem.* **1982**, *32*.

(10) Pauling, L. *J. Am. Chem. Soc.* **1947**, *69*, 542.

distorted square nets of Sn and S atoms, which are interconnected via the axial bonds. Since the axial SnS bonds are hardly affected, we can describe the transformation as bond breaking in square nets of Sn and S atoms to form SnS zigzag chains **7**, which are

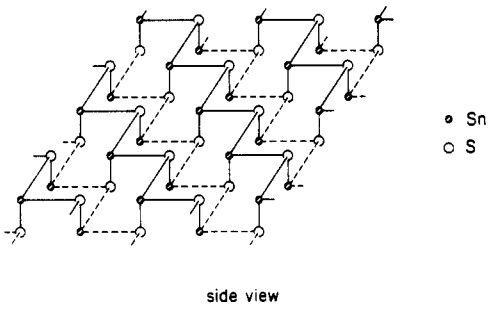

7

interconnected by the axial bonds. From another point of view, SnS layers with lower coordination numbers for Sn and S are formed.

We have built up substantial experience in the analysis of structures based on square nets, e.g. the $ThCr_2Si_2$,[11] $BaAl_4$,[12] and $CaBe_2Ge_2$[13] phases as well as PbO,[14] and we have analyzed geometrically similar distortions in ZrSiS, $ZrSi_2$, and ATB_2 materials (A = alkaline-earth metal, La; T = Mn, Co, Cu, Zn; B = Sb, Bi).[15] Structural maps for 10-electron compounds have been presented by various authors.[16] We will use some of that experience in our analysis of the SnS phase transformation. It should be mentioned that previous calculations and XPS studies on the GeS modification of SnS exist in the literature.[17] Our computations are of the extended Hückel type with details provided in the Appendix.

Building Up the SnS (TII) Electronic Structure

The simplest starting point to build up the SnS band structure in the TII form is a diatomic SnS monomer. An interaction diagram is shown in Figure 1. The lowest orbital is essentially sulfur 3s with a small amount of Sn 5p mixed in. Next, there is the σ or σ^* combination of 5s (Sn), with the two lone pairs between them. The bonding essentially results from a partial electron transfer from Sn to S.

Next we move to an idealized two-dimensional layer, which was shown in two different views in **6**. The actual structure is orthorhombic (space group *Cmcm*), but the lattice constants *a* and *c* are very similar. So we will assume for the moment a tetragonal

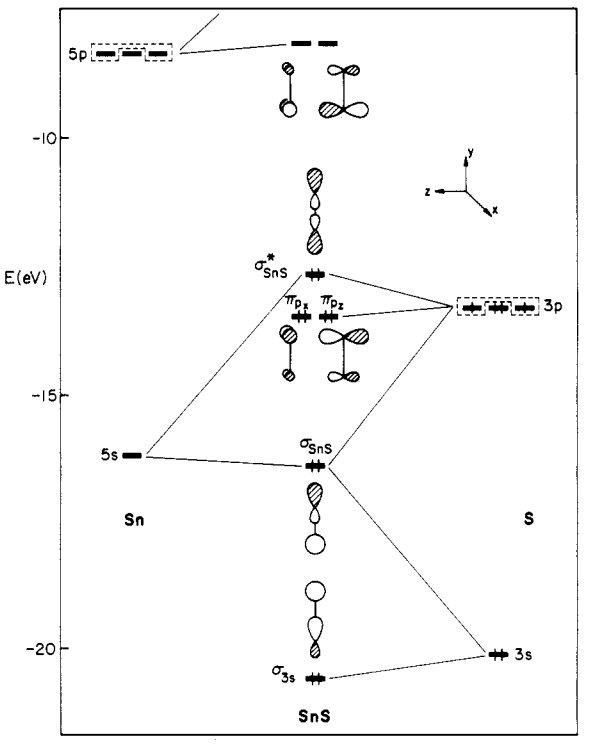

Figure 1. Interaction diagram of Sn and S to form a SnS monomer.

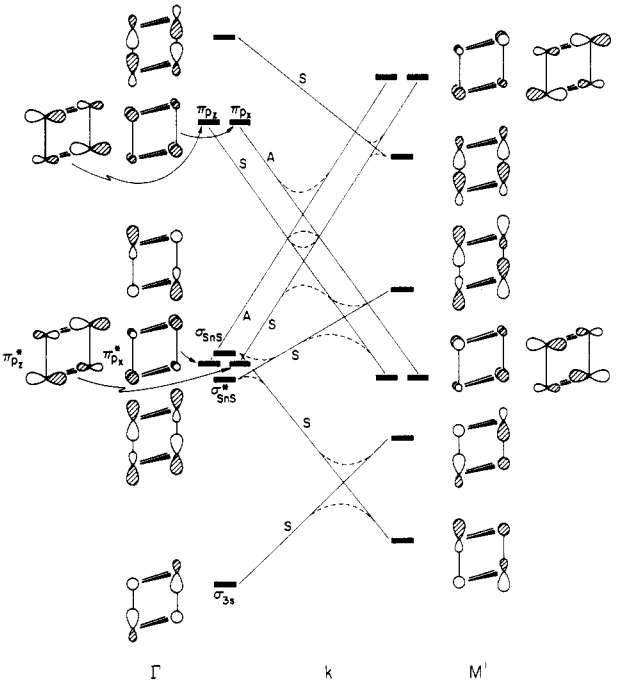

Figure 2. Schematic 2D band structure for SnS (TII modification) along Γ–M′, using a glide plane as translation unit. Dashed lines indicate the shape bands would have without mixing.

structure to simplify the analysis. In the solid, each SnS unit in an upright position is surrounded by four nearest-neighbor units pointing down. In the primitive unit cell, the first SnS unit in Figure 2 is related to the second unit by an *n* glide plane. A schematic representation of the primitive unit cell and the corresponding Brillouin zone is given in **8** and **9**. What we do here to derive the band structure is to use the maximum symmetry available, in particular, the glide plane symmetry. This reduces the number of bands to eight. The complete band structure may be generated later by a back-folding procedure, which projects areas or lines of the larger Brillouin zone for one SnS per asymmetric unit (that we use here) into the smaller Brillouin zone for the conventional SnS cell (which is half as large, since we have

(11) Zheng, C.; Hoffmann, R. *J. Phys. Chem.* **1985**, *89*, 4175.
(12) Zheng, C.; Hoffmann, R. *Z. Naturforsch., B: Anorg. Chem., Org. Chem.* **1986**, *41B*, 292.
(13) Zheng, C.; Hoffmann, R. *J. Am. Chem. Soc.* **1986**, *108*, 3078.
(14) Trinquier, G.; Hoffmann, R. *J. Phys. Chem.* **1984**, *88*, 6696.
(15) (a) Cordier, G.; Eisenmann, B.; Schäfer, H. *Z. Anorg. Allg. Chem.* **1976**, *426*, 205. (b) Cordier, G.; Schäfer, H. *Z. Naturforsch., B: Anorg. Chem., Org. Chem.* **1977**, *32B*, 383. (c) Brechtel, E.; Cordier, G.; Schäfer, H. *Z. Naturforsch., B: Anorg. Chem., Org. Chem.* **1980**, *35B*, 1. (d) Cordier, G.; Schäfer, H.; Woll, P. *Z. Naturforsch., B: Anorg. Chem., Org. Chem.* **1985**, *40B*, 1097. (e) Brechtel, G.; Cordier, G.; Schäfer, H. *Z. Naturforsch., B: Anorg. Chem., Org. Chem.* **1979**, *34B*, 251. (f) Tremel, W.; Hoffmann, R. *J. Am. Chem. Soc.*, in press.
(16) (a) Kawamura, H. *Comments Solid State Phys.* **1979**, *9*, 55. (b) Zunger, A. *Phys. Rev. B: Condens. Matter* **1980**, *22*, 5839. (c) Littlewood, P. B. *J. Phys. C* **1980**, *13*, 4855, 4875. Gornik, E.; Heinrich, H.; Palmetshofer, L. *Lect. Notes Phys.* **1982**, *152*, 238. (d) Polatoglou, H. M.; Theodorou, G.; Economou, N. A. *Phys. Rev. B: Condens. Matter* **1986**, *33*, 1265. (e) Polatoglou, H. M. *Phys. Rev. B: Condens. Matter* **1986**, *33*, 5865.
(17) Band structure calculations. For SnS: Newmann, H.; Kosakov, A. *Phys. Status Solidi B* **1978**, *B85*, K11. Parke, A. W.; Srivastava, G. P. *Phys. Status Solidi B* **1980**, *B101*, K31. For SnSe: Abbati, I.; Braicovich, L.; Cuicci, B. *Nuovo Cimento Soc. Ital. Fis, B* **1977**, *39B*, 727. For GeS: Grandke, T.; Ley, L. *Phys. Rev. B.: Solid State* **1977**, *16*, 832. For XPS measurements see: Shalvoy, R. B.; Fisher, G. B.; Stiles, P. J. *Phys. Rev. B: Solid State* **1977**, *15*, 202. Kemeny, P. C.; Azoulay, J.; Cardona, M.; Lay, L. *Nuovo Cimento Soc. Ital. Fis, B* **1977**, *39B*, 709. Berg, U.; Chasse, T.; Bruemmer, O. *Phys. Status Solidi* **1981**, *108*, 507.

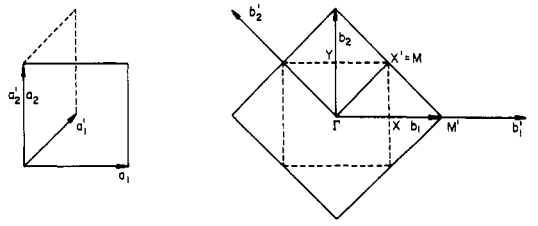

8 9

twice as many atoms). The glide plane band structure will look different from the conventional one due to the fact that we plot the glide plane band structure along a_1' and a simple translation along a_2'.

Let us proceed now to a qualitative construction of the band structure along Γ–M′ in Figure 2. First is the σ_{3s} orbital. At M′ next-nearest-neighbor interactions are antibonding, and so the band rises in energy when moving along the line. At Γ, the σ^*_{SnS} orbital is stabilized by nearest neighbor interactions. At M′, it is slightly destabilized and, therefore, the band goes up in energy along Γ–M′. Likewise, the bands derived from the σ_{SnS} and 4σ (not shown in Figure 2) orbitals of the monomer unit are pushed up in energy at Γ and will be stabilized on going from Γ to M′. The π^* combination is strongly stabilized by nearest-neighbor interaction at Γ; the π combination is substantially destabilized. At M′, the situation is reversed. Due to the π (π^*) bonding character in the monomer unit, the π (π^*) combination ends up at M′ somewhat lower (higher) in energy than the π^* (π) combination started out at Γ. This schematic construction is reflected well in the calculated band structure of Figure 3. Symmetry constraints and resulting avoided crossings are easily taken into account.

How are the primitive and conventional unit cell related? Making use of group theoretical arguments, we can construct the band structure along Γ–X of the conventional unit cell from the band structure (primitive cell) along Γ–M′, given in Figures 2 and 3. The relation between the Brillouin zones of the primitive and conventional lattice was given in **9**. The line Γ–X of the small Brillouin zone (conventional unit cell) can be generated by back-folding the line Γ–M′ in such a way that M coincides with Γ. This means that the bands of the conventional unit cell at Γ can be expressed in terms of bands of the primitive cell at Γ and M′. In fact, a look at Figure 2 reveals that the levels at Γ and M′ are simply the symmetric and antisymmetric combination of the orbitals of the SnS dimer unit. Having done the back folding, we need to drop in the last step our initial assumption of a tetragonal structure and go to the real SnS unit cell. Since $a \approx c$ (with respect to **3**), the band structure along Γ–X and Γ–Z in the 2D Brillouin zone of the real unit cell will be very similar, the only obvious difference being some broken degeneracies at Γ. The SnS band structure (TlI modification) given in Figure 4 is very close to our prediction. As a consequence of the nonsymmorphic symmetry elements, the bands stick together along two symmetry lines in Figure 4.

That finishes the construction of the SnS electronic structure in the TlI modification. The next figure, Figure 5, shows the band structure of the same material in the alternative GeS modification. For the 10-electron compound, SnS, the first 10 bands are filled. Next comes a gap of ~4 eV, (compared to a calculated band gap of 1.0 and 1.8 eV for the three-dimensional structures). The highest occupied band is a lone pair orbital on Sn in both structure types. It is repulsion between these lone pairs that is responsible for the breakup of the NaCl structure. Since the orbital is sticking out of the layer, it will be perturbed by the stacking of the 2D slabs. However, as we will see, it is the in-plane orbitals that are responsible for the observed distortion from one structure to the other. For the derivation of an orbital picture of the phase transition, we may benefit again from an understanding of the symmetry properties of the process. These are summarized by the space group transformation

$$C2/m2/c2_1/m \xrightarrow{k2} P2_1/b2_1/n2_1/m$$

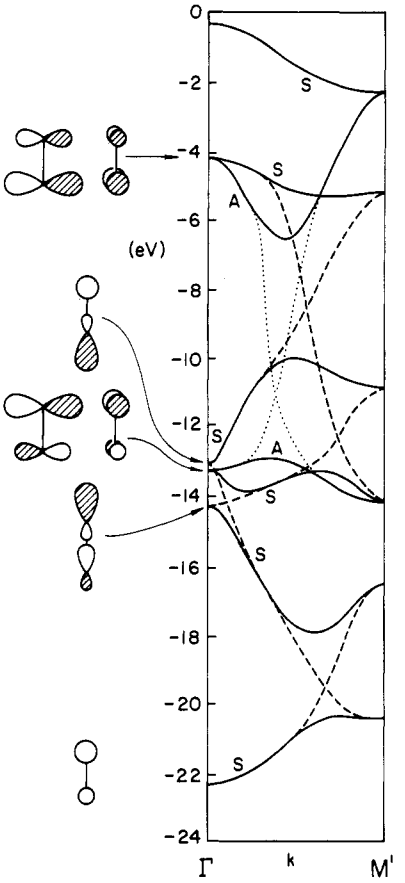

Figure 3. Calculated 2D band structure for SnS (TlI modification) along Γ–M′. Dashed and dotted lines indicate the shape bands would have without mixing.

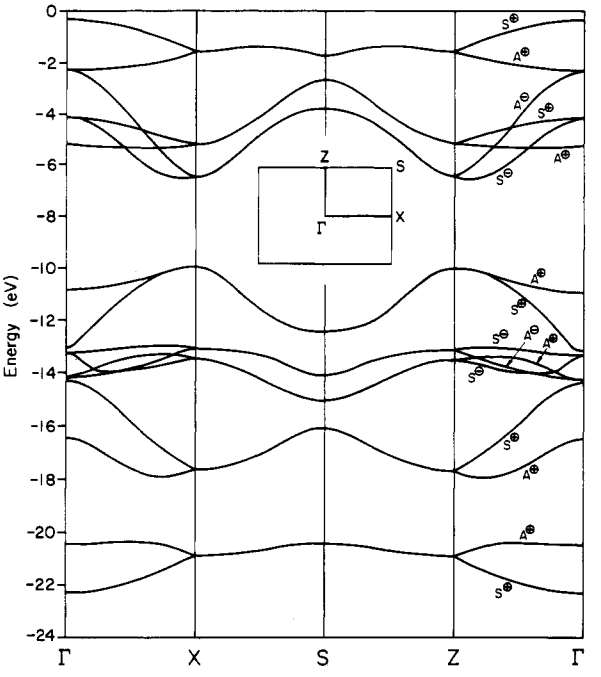

Figure 4. 2D band structure of SnS (TlI modification).

In this "klassengleich" transition, we lose a number of symmetry elements and shift the origin by $^1/_4$, $^1/_4$, 0. The pivotal symmetry element lost is a mirror plane. Our discussion did not yet include the lost translations. In going from the space group *Cmcm* to *Pbnm*, $T = m\vec{a} + n\vec{b} + p\vec{c}$ remain, but $T = (m + {}^1/_2)\vec{a} + (n + {}^1/_2)\vec{b} + p\vec{c}$ are lost. This implies that the transition corresponds to $k = \vec{a}^*$, and this makes the connection to a Peierls distortion. $k = \vec{a}^*$ identifies the wave vector of a soft phonon mode. The

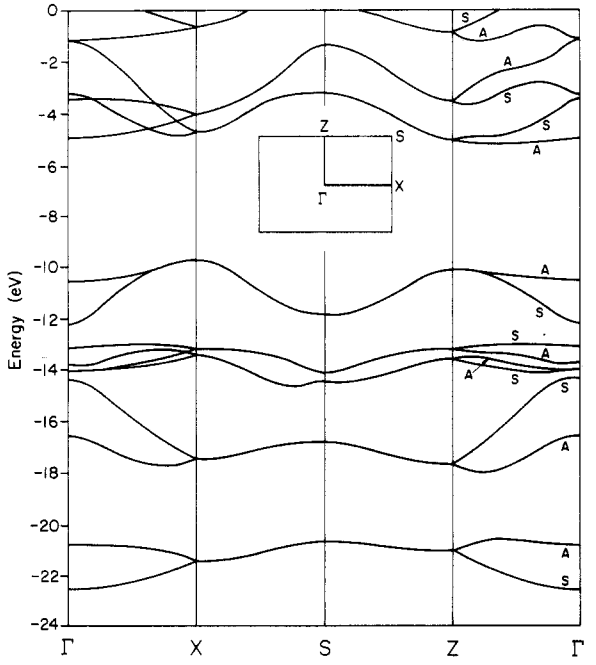

Figure 5. 2D band structure of SnS (GeS modification).

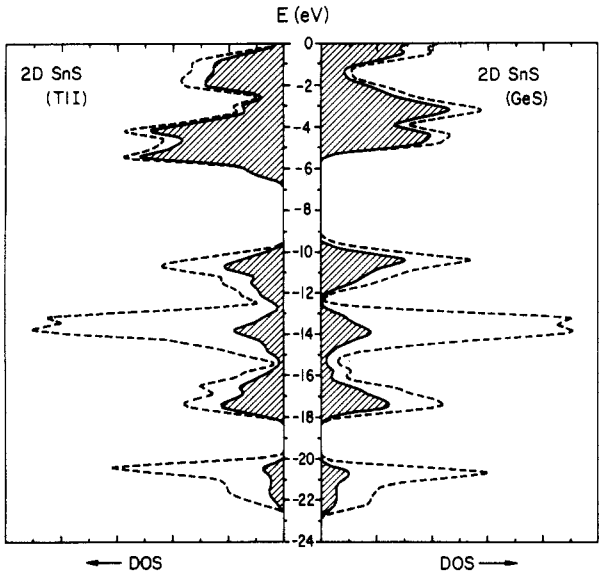

Figure 6. Total DOS (dashed line) and Sn contribution (solid line) for the 2D SnS structures: left, TII modification; right, GeS modification.

orbitals involved in the bond breaking are localized in the layer plane or at least have a substantial in-plane component. The band gap increases a little on distortion. Examination of the densities of states in the structures (Figure 6) shows that some states have been pushed up and some are stabilized, but the overall effect is small. It is not surprising that this is a second-order phase transition.

Though the effect is small, we think we can still trace the deformation to a familiar cause: due to the loss of symmetry elements, some bands may mix. We have the analogue of a second-order Jahn–Teller effect in the solid.

From the picture of the two structures in **3**, it is obvious that the mirror plane present in the *bc* plane of the high-symmetry structure is lost. Therefore, orbitals that were symmetric and antisymmetric with respect to this symmetry element before are now allowed to mix. The important symmetry line is Γ–Z, and we examine the orbitals at Z, where they are real. Each band is represented at Z by a degenerate pair of crystal orbitals. The symmetry along this line is C_{2v} in the high-symmetry structure, but only C_2 in the distorted structure. The symmetry levels S/A refer to the 2_1 screw axis; + and − refer to the mirror plane in the undistorted structure. From Figures 4 and 5, it is apparent that the band pairs 11, 12 and 13, 14 above the Fermi level are most affected, and from perturbation theory we know that these bands mix into the lower bands in a bonding fashion. The in-plane contributions of band pairs 9, 10 and 11, 12 are shown in Figure 7 in a top view on the SnS layer. In parts a and b of Figure 7, we draw the orbitals of the top layer; in parts d and e of Figure 7, those of the bottom layer are drawn. The pairs 9, 10 and 11, 12 have different symmetries in the undistorted structure. In the distorted structure, the symmetry is the same and the bands are allowed to mix. This process is shown for the bonding combination of top and bottom layers in parts c and f of Figure 7. Band pairs 9, 10 and 11, 12 are not the only candidates for mixing; the combinations 5, 6 and 13, 14 given in a side view in **10** and **11**

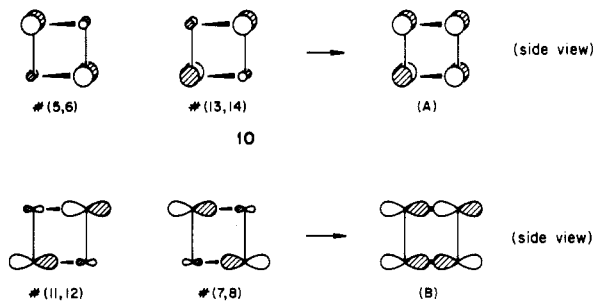

certainly meet the symmetry requirements as well. In fact, all of these combinations mix. We are not going through all the details of this process; mixing of band pairs 13, 14 and 5, 6, and 11, 12 and 7, 8, respectively, as shown in a side view in **10** and **11**, equilibrates the coefficients on Sn and S approximately. **10** and **11** can be combined to the wave function for band pair 5, 6 of the distorted structure, shown in a side view in **12** and in a top view on the top and bottom layer in **13** and **14**.

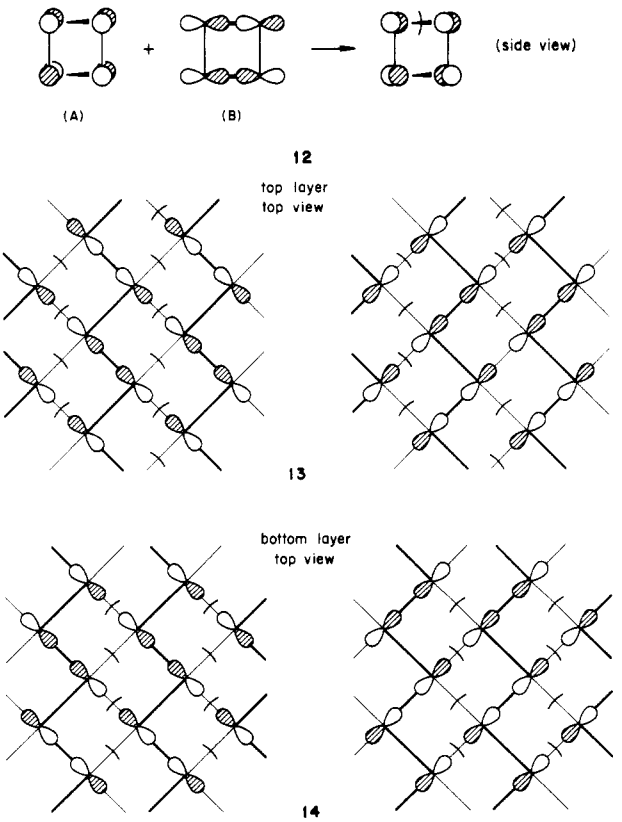

We mentioned already that the phase transition can be described equally well as a Peierls type transition, and we identified the corresponding *k* vector. In the 3D structures **3** the "doubling" of the unit cell is connected to the loss of a twofold axis C_{2x} (x, 0, 0) in the phase transition. In the 2D structures, we do not have

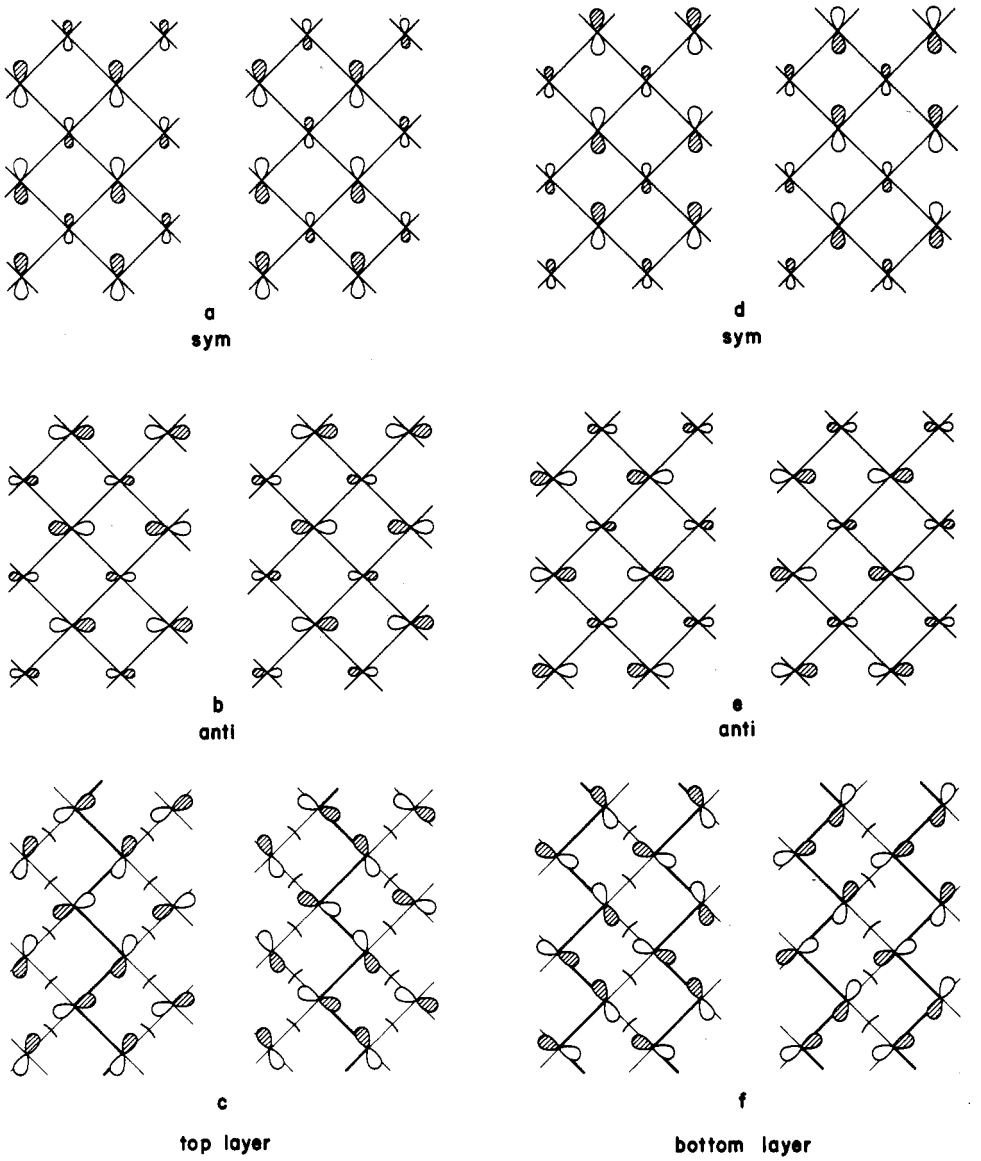

Figure 7. Crystal orbitals of a 2D layer at Z, relevant to the TlI–GeS distortion, shown in a top view (only the in-plane component is shown): left, top layer; right, bottom layer. The crystal orbitals are symmetric and antisymmetric with respect to a mirror plane as indicated in parts a and d. The symmetric combinations a and d are not allowed to mix with the antisymmetric combinations b and e in the high-symmetry TlI structure type. In the absence of the mirror plane in the low-symmetry GeS structure, however, both crystal orbitals mix, resulting in a stabilized (parts c, f) and destabilized (not shown) combination.

a symmetry restriction that prevents bands from mixing in the TlI modification but not in the GeS polymorph. However, a glimpse at the band structures in Figures 4 and 5 shows that the band gap widens considerably at X. The reason can easily be rationalized from an orbital picture. At X, each band is represented by a degenerate pair of crystal orbitals. In **15** and **16**, we

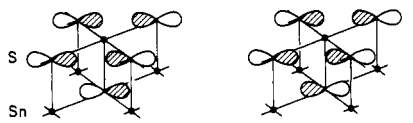

15

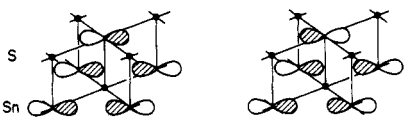

16

show the orbitals for pairs 9, 10 and 13, 14 (TlI modification) at X. For reasons of clarity, only the in-plane component is given. In the undistorted structure we observe only a negligible amount of mixing of these two combinations. In the distorted structure, however, the mixing is substantial. This is shown in **17a**,**b**. In

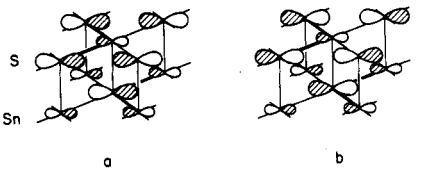

17

the distorted geometry, one of these combinations (**17a**) is stabilized; the other one (**17b**) is pushed up in energy. The picture is, therefore, analogous to a pairing distortion, the prototype being a linear chain of hydrogen atoms that distorts to diatomic molecules.

The net result is a distortion from the TlI to the GeS structure. Since as many bonds are broken in the transition as are formed, we expect the resulting energy change to be small. In the 2D calculations, we favor the low-symmetry structure by 0.135 eV per formula unit. For the experimental 3D structure the TlI

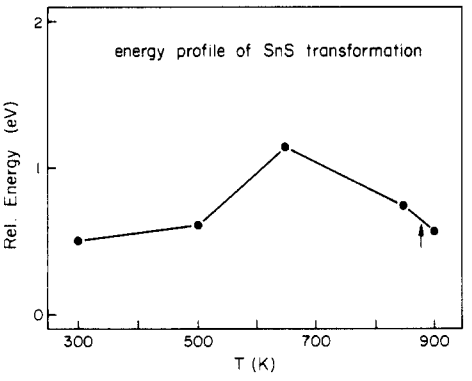

Figure 8. Energy profile for the SnS transformation, 3D structure. The arrow indicates the transition temperature.

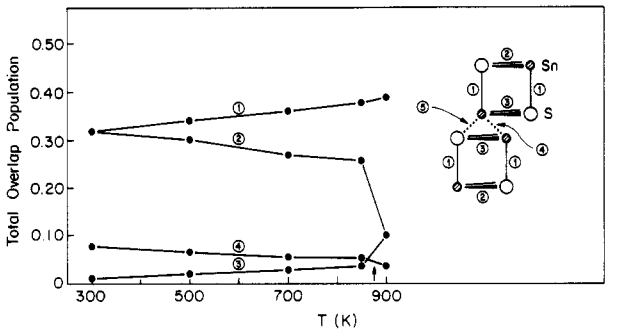

Figure 9. Evolution of some overlap populations for the 3D structures in the SnS transformation. The arrow indicates the transition temperature.

modification is preferred by 0.05 eV.

The experimental neutron diffraction studies[9d] give us structural parameters as a function of temperature. If we use these as input for our calculations, we obtain the energy profile of Figure 8. Keeping in mind that that extended Hückel procedure is not especially reliable for bond extensions, the best we can say is that the energy profile for the reaction is soft. The changes in the overlap populations during the reaction are plotted in Figure 9. The changes from 300 to 850 K are very small, and only in the temperature interval between 850 and 900 K is a drastic change in the overlap population of the basal SnS bonds observed. The pictorial interpretation is a sudden weakening of this bond, a phonon soft mode in the physicist's jargon.[18]

Let us restate our conclusion: *The reason for the TlI → GeS transformation is a mixing of the conduction band into the valence band.* This conclusion can be generalized and applied to other examples. As we move from the light to the heavier elements of a group in the periodic table, the elements become more metallic or more electropositive. The consequence in the present case is an increased "band gap" for SnS compared to GeS. A larger "band gap" again means less effective mixing. Therefore SnS has less tendency to distort. For GeS the "band gap" is smaller, the mixing is more effective, and consequently only the distorted low-symmetry structure is observed. In TlI itself, the "gap" between the valence and conduction bands is still larger than in SnS. Little mixing can occur, and the undistorted structure exists, leaving SnS as an intermediate case where both the undistorted and distorted structures can be adopted. The experimentally determined optical band gaps in GeS and SnS are approximately 1.6[19] and 1.2 eV,[20] which seems to indicate the opposite trend. We think, however, that this contradiction can be resolved. The word "gap" as we used it in this connection should refer to the energy difference between the π and π^* type states in the solid-state materials. These are clearly the "in-plane" orbitals (p_x and p_z in our coordinate system), which are responsible for making and breaking the bonds in question. In the interaction diagram in Figure 2, these orbitals are easily identified. With application of the electronegativity argument, the π^* orbitals move to higher energies if one moves from Ge to Sn and Tl. Given a constant anion, the π orbitals stay at approximately the same energy.

In the solid-state materials, these orbitals spread out into bands, but the basic featurs of the dimer building block are still preserved. We could see this by comparing the tentative band structure in Figure 2 with its calculated counterpart in Figure 3.

A word about the electronegativity differences is still in order. The EN differences we are talking about are quite small (for Tl, Ge, and Sn, EN = 2.0; for S and Se, EN = 2.6; For I, EN = 2.7[21]). Whereas for TlI the EN values immediately support a more ionic model and a larger "gap", one is not able to differentiate between GeS and SnS based on Pauling's EN scale. A number of well-known facts (e.g. gray and white Sn modifications, trends in ionization enthalpies, etc.),[22] however, show that Sn actually is more metallic than Ge.

Similar reasoning can be applied for the tellurides. The GeTe structure,[4] which is an ordered variant of the rhombohedral As structure,[3] undergoes at 400 °C a transition to a rock salt structure type. In fact, the GeTe structure can be derived from the parent rock salt structure, just like the GeS structure type, by breaking three mutually orthogonal linkages around each octahedrally coordinated rock salt site.[2] Black phosphorus has been reported to undergo a phase transition at 50 kbar to the A7 arsenic structure.[7] We do not want to dwell on this particular point, since this has been analyzed by Burdett and co-workers[23] in some detail.

What about the lead chalcogenides? Let us recall that the action of the lone pair in 10-electron compounds causes a breaking of bonds in the rock salt parent structure, resulting in typical 10-electron structure types, such as TlI or GeS. For lead and other heavy elements, relativistic effects are well-known to contract the 5s orbital and to lower its energy.[24] This is generally known as the inert-electron-pair effect. As a result, the lone pair repulsion in lead chalcogenides, e.g. PbS, is reduced and a rock salt structure is preferred.

One point still to be considered is the stacking of the 2D layer to the full three-dimensional structure. A detailed discussion of interlayer bonding in 10e compounds has been given by Trinquier and one of us[14] in our analysis of PbO. We want to highlight only a few points here. When the layers are stacked together, the bands that have lobes pointing away from the layer will be perturbed. In simple terms, a symmetric and antisymmetric combination of these orbitals can be formed. This is shown schematically in a projection on the layers in **18** and **19**. At the Γ point, the symmetric combination will be stabilized, the antisymmetric combination will be destabilized. Going along the different symmetry lines, we can predict the evolution of the bands from the phase of the lobes pointing up and down. We will not pursue this in further detail here, but the general result is a broadening of the highest occupied bands. We can pick up these features in the DOS curves for the GeS and TlI modification, but do not show those curves here.

For the experimental geometries, we calculate net charges of 0.98 (TlI) and 0.82 (GeS) on each tin atom. The resulting Sn–Sn

(18) Megaw, H. D. *Crystal Structures: A Working Approach*; Saunders: Philadelphia, 1973; p 453.

(19) (a) Wiley, J. D.; Breitschwerdt, A.; Schönherr, E. *Solid State Commun.* **1975**, *17*, 355. (b) Eymard, R.; Otto, A. *Phys. Rev. B: Solid State* **1977**, *16*, 1616. (c) Lukeš, F.; Schmidt, E.; Lacina, A. *Solid State Commun.* **1981**, *39*, 921. (d) Akimchenko, I. P.; Rasulova, G. K.; Závětová, M. *Czech. J. Phys.* **1981**, *B31*, 687. (e) Pajasova, L.; Vorliček, V.; Zářetová, M.; Štěpánek, B.; Pavlov, S. K. *Czech. J. Phys.* **1983**, *B33*, 101.

(20) (a) Lambros, A. P.; Geraleas, D.; Economou, N. A. *J. Phys. Chem. Solids* **1974**, *35*, 537. (b) Lukeš, F.; Humliček, J.; Schmidt, E. *Solid State Commun.* **1983**, *45*, 445.

(21) Pauling, L. *The Nature of the Chemical Bond*, 3rd ed.; Cornell University Press: Ithaca, NY, 1960; p 93.

(22) Cotton, F. A.; Wilkinson, G. *Advanced Inorganic Chemistry*, 4th ed.; Wiley: New York, 1980; p 374.

(23) (a) Burdett, J. K.; Price, S. L. *Phys. Rev. B: Condens. Matter* **1982**, *25*, 5778. (b) Burdett, J. L.; Lee, S. *J. Solid State Chem.* **1982**, *44*, 415.

(24) (a) Pitzer, K. S. *Acc. Chem. Res.* **1979**, *12*, 271. (b) Pyykkö, P.; Desclaux, J.-P. *Acc. Chem. Res.* **1979**, *12*, 276.

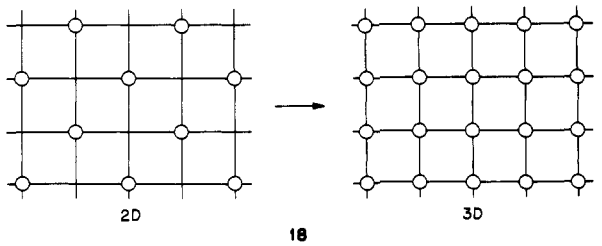

18

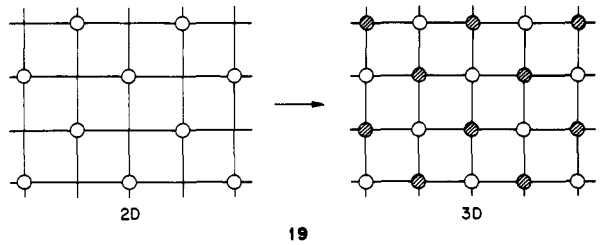

19

overlap populations are 0.073 and 0.046 for interlayer distances of 3.455 and 3.405 Å, respectively. These numbers indicate that there is bonding to some degree between the Sn atoms of different layers. The corresponding COOP curves for intralayer Sn–S and interlayer Sn–Sn bonding are depicted in Figure 10. The lower bands up to −12 eV contribute to Sn–Sn bonding, whereas those above make an antibonding contribution. Contributions to Sn–Sn interlayer bonding will come from orbitals that point into the interlayer region. There are some low-energy bands with this characteristic, but the primary contribution to Sn–Sn bonding comes from the two highest bands. In these bands, in the region −9 to −13 eV, the lower portion is interlayer Sn–Sn bonding, with the upper portion antibonding. This pattern for the overlap population is similar to what has been observed in the PbO case, and we think that it describes the typical bonding situation in ten electron MX compounds.

The evolution of the overlap populations and the relative variation in the total energy when the layers are progressively brought together are shown for the TlI modification in Figure 11. The largest change in the overlap populations corresponds to the interlayer Sn–Sn bond. The overlap population increases strongly if the layers are pressed together beyond the experimental distance. The intralayer Sn–S overlap populations decrease during this process; the intralayer Sn–Sn overlap population is negative and very small. The same holds for interlayer Sn–S and S–S overlap populations. The interaction between the layers is repulsive, as can be seen from the energy variation. The experimental geometry (b = 11.48 Å) is on the softly rising part of the energy curve.

Let us conclude this section with a brief comparison of the SnS structure types with the PbO structures, which were analyzed by Trinquier and one of us previously.[14] PbO exists in tw polymorphic forms: red tetragonal α-PbO (litharge) and yellow orthorhombic β-PbO (massicot). Both structures are layer structures with 10 electrons per formula unit as SnS. Although the atoms in PbO are four-coordinated (instead of five-coordinated as in SnS), the bonding picture in PbO and SnS is—even up to finer details—remarkably similar. Some of the points were mentioned in the text. Transitions between both PbO forms have been reported,[25] but although they are "symmetry-allowed" (first Landau condition),[9] they are not of second order type.

Interestingly enough, we encounter the double layers observed in the TlI structure in the intercalation compound $(Te_2)_2I_2$[25] (**20**) again. This truly remarkable material contains planar double layers of tellurium formed from Te_2 units (if we follow the hierarchy of interactions), which are arranged along the c axis. As in the TlI structure, this provides a 1 + 4 coordination for the Te atoms with Te–Te distances of 2.713 and 3.323 Å. Monomolecular planar layers of I_2 molecules are situated between the

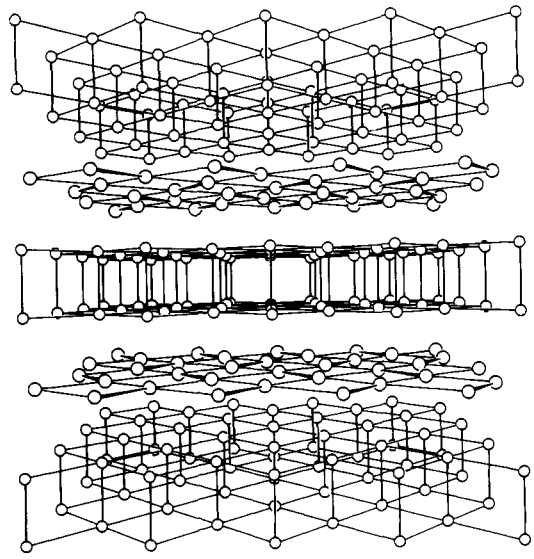

20

layers, the intramolecular bond length being 2.715 Å and the intermolecular contacts being more than 3.384 Å. Can we expect a distortion of the Te double layers similar to that observed in SnS?

On the basis of the experience we have accumulated up to this point, we can predict qualitatively the shape of the band structure of a Te 2D double layer. Since the geometries of the SnS (TlI) and Te_2 layers are very similar, we expect the shape of the bands to be alike in both cases. The important difference originates from the atom electronegativities. The interaction diagram in Figure 2 shows that the Sn- and S-centered orbitals are nicely separated, due to the different electronegativities of Sn and S. The orbitals for the Te_2 fragment in **21** are those of a homonuclear diatomic

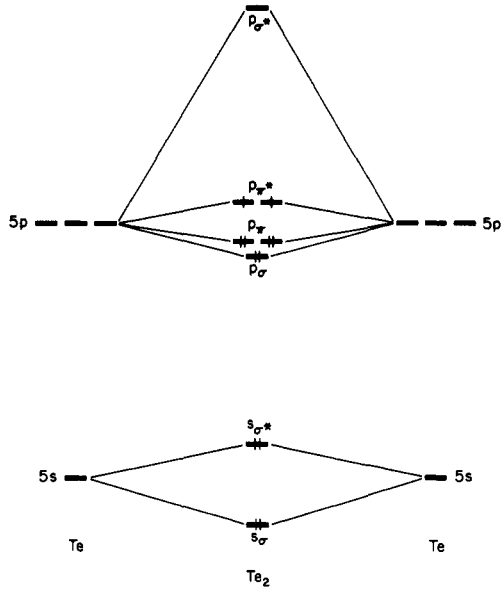

21

unit. The level ordering is the familiar σ, π, π^*, σ^* sequence, and the splitting of the p_{π} levels is ~6 eV, the p_{σ} splitting being ~14 eV for the given Te–Te distance.

In the next step the Te_2 units are arranged to form a double layer, and the orbitals of the molecular unit spread out into bands. The p_{σ} bands have only a small overlap along any direction in the two-dimensional Brillouin zone. Therefore the resulting bands have to be rather flat. The p_{π} orbitals, however, show substantial overlap, and the bands will show large dispersion. The situation is very similar to that for a square net of atoms. Because we discuss a double layer of atoms, the number of bands simply has

(25) Okuri, Y.; Ogo, Y. *Bull. Chem. Soc. Jpn.* **1982**, *55*, 3641.
(26) Kniep, R.; Beister, H.-J. *Angew. Chem.* **1985**, *97*, 399; *Angew. Chem., Int. Ed. Engl.* **1985**, *24*, 394.

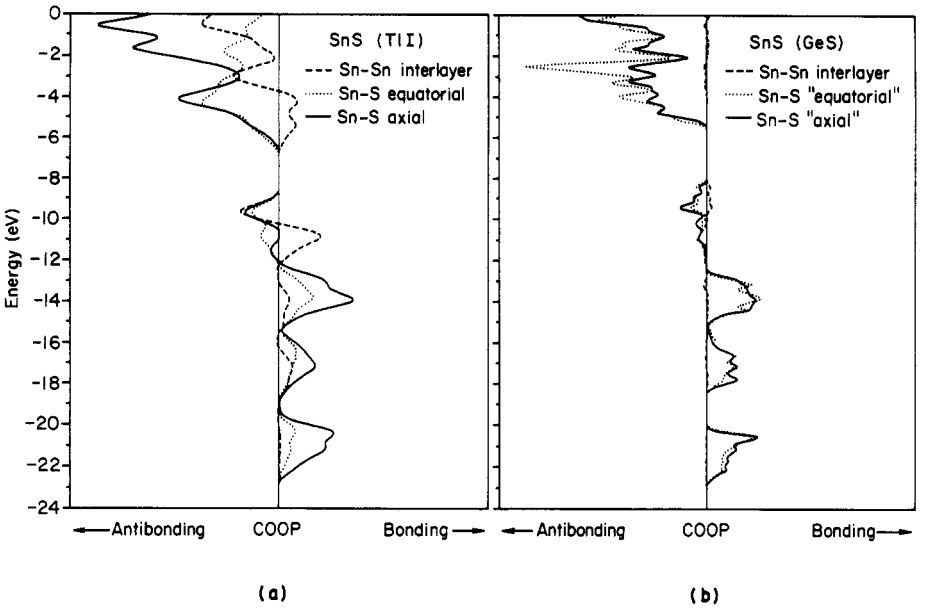

Figure 10. COOP curves showing axial intralayer Sn–S bonding (solid line) and interlayer Sn–Sn bonding (dashed line): left, TlI modification; right, GeS modification.

to be doubled by forming a symmetric and antisymmetric combination. The calculated band structure is shown in Figure 12. There is a striking similarity to the band structure of SnS in the TlI modification; only the dispersion of the bands has changed. Let us discuss the band composition at Γ. The lowest four bands are the 5s bands. Bands 5 and 8 (**22** and **23**) are one of the π/π^*

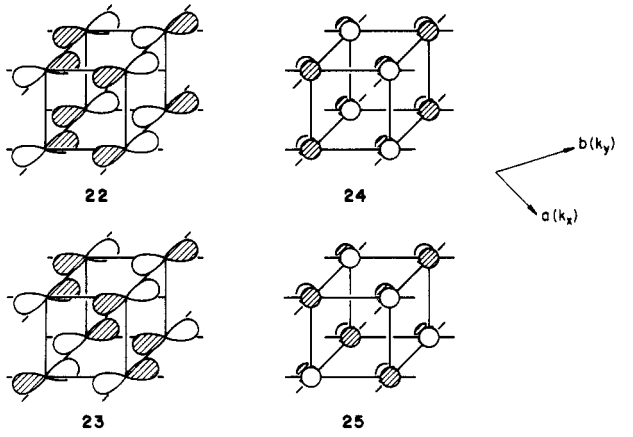

combinations of the Te_2 fragment; they are bonding between the Te_2 units. The other π/π^* combination, which is bonding between the Te_2 units, is composed of bands 7 and 9 (**24** and **25**). Bands 11/13 and 12/14 are the corresponding antibonding partners. These bands are involved in the basal bonding around Te. The p_σ combination (now bonding within but bonding and antibonding between Te_2 fragments), which is involved in the axial bonding, is given in bands 6 and 10 (**26** and **27**). The highest two bands,

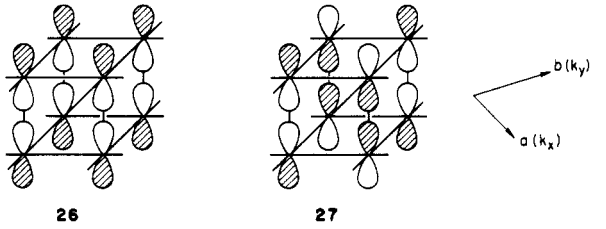

bands 15 and 16, are the corresponding antibonding partners (p_{σ^*}, antibonding within and bonding/antibonding between the Te_2 units).

For Te double layers we have 24e/unit cell (12e/Te_2), and the corresponding Fermi level is indicated by an arrow at the left margin of Figure 12. Since the p bands overlap very efficiently,

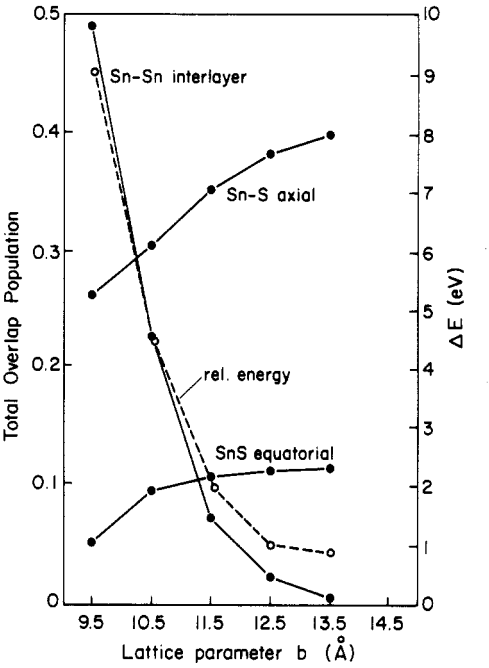

Figure 11. Evolution of some overlap populations (solid lines) and the total energy (dashed line) as a function of the stacking of the layers in SnS (TlI modification). The interlayer distance is the vector $b/2$ of the direct lattice.

Table I. Extended Hückel Parameters

orbitals		H_{ii}, eV	ζ
Sn	5s	−16.16	2.32
	5p	−8.32	1.94
S	3s	−20.00	2.12
	3p	−13.30	1.83
Te	5s	−20.78	2.57
	5p	−14.80	2.16

for the given electron count a distortion of the Te double layer to a GeS type structure is not likely to provide a significant stabilization.

Let us discuss qualitatively what happens when I_2 is intercalated between the Te double layers. The intramolecular I–I distance of 2.713 Å is close to the 2.66 Å value found in molecular I_2, and therefore the iodine-centered bands are likely to be very narrow.

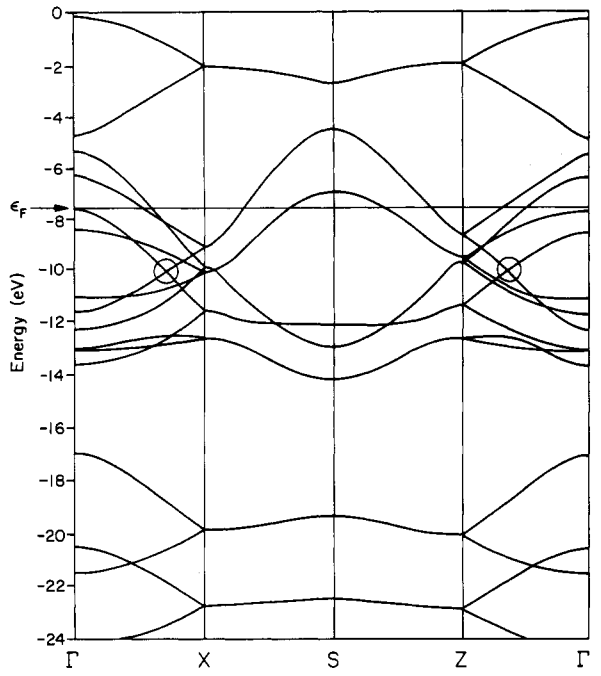

Figure 12. Band structure of a 2-dimensional Te_2 slab.

Since iodine is more electronegative than tellurium, some charge transfer from Te to I–I antibonding states is bound to occur, resulting in a weakening of the I–I bond and a lowering of the Fermi level compared to the Te double layer. In fact the I–I bond distance is slightly longer than the reported distance in molecular I_2.[27] A distortion of the Te layers, however, is not likely to occur. This becomes clear from the position of the crucial band crossings (circled in Figure 12), which are deeply buried in the 5p bands. Our calculations indicate a distortion of the Te double layer as possible for an electron count of less than 20e/unit cell. Therefore for any halogen-intercalated material the general structure of the Te_2 slabs would remain unchanged.

It may be worthwhile to mention here also the structural relationships between the TlI and CrB structure[28] (**28a**) and the GeS and FeB structure[29] (**28b**). There are only small differences

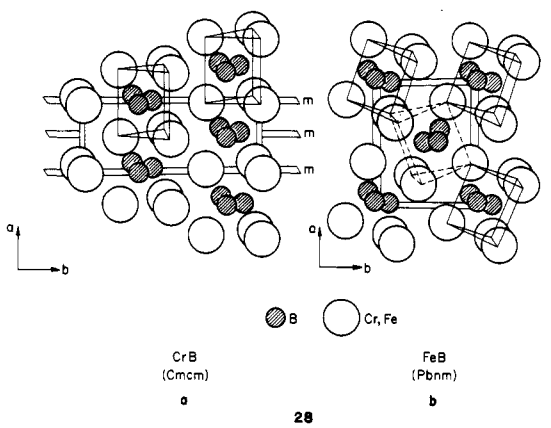

28

in the structural parameters, leading to a B–B zigzag chain in the CrB and FeB structures. Interestingly (since our arguments are mainly symmetry-based) the symmetry relationship between the undistorted CrB and distorted FeB structures is similar to that for the TlI and GeS case. Binary borides adopt one of these two structure types depending on the electron count.[30]

Whereas the Te double layer in $(Te_2)_2I_2$ could be related to the SnS (TlI) structure by adding two electrons, one may equally well want to remove one electron (on paper). This leaves us with the nine-electron compounds, and the unpaired electron is taken care of by connecting two layers by a metal–metal bond, as in GaS.[31] Alternatively one can break a bond in the NaCl structure, a nice example being GeP.[32] In InS[33] (**29b**) two GeS type layers

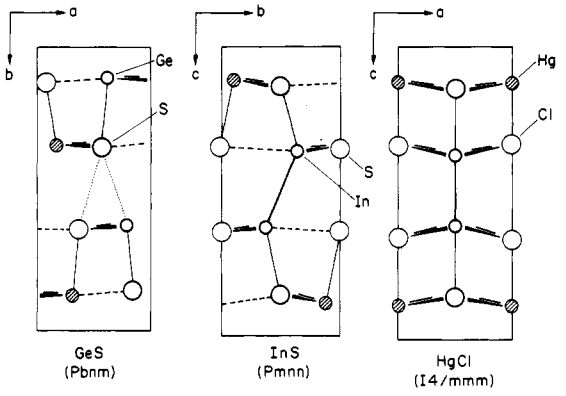

29

(GeS given in **29a** for comparison) are connected by an In–In bond. A corresponding high-symmetry version (due to the missing lone pair) is found in the tetragonal HgCl structure[34] (**29c**), where a Hg–Hg bond is formed.

Acknowledgment. W.T. thanks Ralph Wheeler and Chong Zheng for helpful discussions. We are also grateful to two knowledgeable reviewers for helpful comments. The stay of W.T. at Cornell was made possible by fellowships from DAAD/NATO and the Deutsche Forschungsgemeinschaft (DFG). Our research at Cornell was generously supported by the National Science Foundation through research Grant DMR821722702 to the Materials Science Center. We are grateful to Christine Gray and Linda Kapitany for the typing, and to Jane Jorgensen and Elisabeth Fields for their expert drawings.

Appendix

The extended Hückel method[35,36] in the tight-binding approximation[37] was used in all calculations. The parameters are listed in Table I. For Sn the exponents were contracted to match the experimental band structure,[38] in particular the dispersion along the line Γ–X and at the Γ point. Sets of 27 or more k points were chosen according to ref 39 to calculate the DOS and COOP curves.

Registry No. SnS, 1314-95-0.

(27) Kitaigorodskii, A. I.; Khotsyanova, T. L.; Struchkov, Yu. T. *Zh. Fiz. Khim.* **1953**, *27*, 780.
(28) Kiessling, R. *Acta Chem. Scand.* **1949**, *3*, 595.
(29) Bjurstrøm, T.; Arnfelt, H. *Z. Phys. Chem., Abt. B* **1929**, *B4*, 469.
(30) Wheeler, R. A.; Hoffmann, R., unpublished results.
(31) Hahn, H.; Frank, G. *Z. Anorg. Allg. Chem.* **1955**, *278*, 340. For β-GaSe see: Hahn, H. *Angew. Chem.* **1953**, *65*, 238. For β,γ-GaSe see: Jellinek, F.; Hahn, H. *Z. Naturforsch., B: Anorg. Chem., Org. Chem.* **1961**, *16*, 713. For γ,ε-GaSe see: Schubert, K.; Dörre, E.; Kluge, M. *Z. Metallkd.* **1955**, *46*, 216. For δ-GaSe see: Kuhn, A.; Chevalier, R.; Rimsky, A. *Acta Crystallogr., Sect. B: Struct. Crystallogr. Cryst. Chem.* **1975**, *B31*, 2841.
(32) (a) Donohue, P. C.; Young, H. S. *J. Solid State Chem.* **1970**, *1*, 143. (b) Bularzik, J. H.; Burdett, J. K.; McLarnan, T. J. *Inorg. Chem.* **1982**, *21*, 1434.
(33) Schubert, K.; Dörre, E.; Günzel, E. *Naturwissenschaften* **1954**, *41*, 448.
(34) Dorm, E. *J. Chem. Soc., Chem. Commun.* **1971**, 466.
(35) Hoffmann, R. *J. Chem. Phys.* **1963**, *64*, 1397. Hoffmann, R.; Lipscomb, W. M. *Ibid.* **1963**, *36*, 3179, 3489; **1962**, *37*, 2872.
(36) Ammeter, J. H.; Bürgi, H.-B.; Thibeault, J. C.; Hoffmann, R. *J. Am. Chem. Soc.* **1978**, *100*, 3686.
(37) (a) Whangbo, M.-H.; Hoffmann, R. *J. Am. Chem. Soc.* **1978**, *100*, 6093. (b) Whangbo, M.-H.; Hoffmann, R.; Woodward, R. B. *Proc. R. Soc. London, A* **1979**, *366*, 23.
(38) Höchst, H.; Hernandez-Calderon, I. *Surf. Sci.* **1983**, *126*, 25.
(39) Pack, J. D.; Monkhorst, J. H. *Phys. Rev. B: Solid State* **1977**, *16*, 1748.
(40) The periodic group notation in parentheses is in accord with recent actions by IUPAC and ACS nomenclature committees. A and B notation is eliminated because of wide confusion. Groups IA and IIA become groups 1 and 2. The d-transition elements comprise groups 3 through 12, and the p-block elements comprise groups 13 through 18. (Note that the former Roman number designation is preserved in the last digit of the new numbering: e.g., III → 3 and 13.)